Probing LO phonons of graphene under tension via the $2D'$ Raman mode

Rohit Narula* and Stephanie Reich
Fachbereich Physik, Freie Universität Berlin, Arnimallee 14, Berlin 14195, Germany
(Received 7 February 2013; revised manuscript received 28 February 2013; published 19 March 2013)

We use *ab initio* simulations and perturbation theory to study the $2D'$ Raman mode of graphene subject to biaxial and uniaxial strains up to 2%. We demonstrate that $2D'$ Raman measurements, as a function of polarization and laser energy E_L, can probe the LO phonons of graphene with arbitrary radial and angular extent around Γ. The $2D'$ profile is highly sensitive to uniaxial strain and depends on both polarization and strain orientation. The Grüneisen parameter $\gamma_{2D'} \approx 1.71$ has a mild dependency on the laser energy E_L, and is found to be in good agreement with experiments and comparable in value to γ_G. The shear deformation potential $\beta_{2D'}$ depends strongly on the polarization and strain orientation, becoming negative when the polarizer and analyzer are perpendicular to each other. Finally, we describe a robust method to determine the uniaxial strain by relying solely on polarized measurements of the $2D'$ mode.

DOI: 10.1103/PhysRevB.87.115424 PACS number(s): 81.05.ue, 78.67.Wj, 63.22.Rc

I. INTRODUCTION

Raman spectroscopy has established itself as a workhorse for characterizing graphitic materials.[1,2] With the advent of graphene,[3,4] a flurry of theoretical and experimental activity involving Raman spectra has illumined numerous aspects of fundamental and practical interest. A small selection might include the determination of the number of graphene layers,[2] doping,[5] phonon dispersion mapping,[6,7] phonon anharmonicities,[8] and the measurement of strain and crystalline orientation.[9,10] sp^2 materials are somewhat unique since they provide a number of prominent second-order Raman spectra, for, e.g., the defect-induced D and D' modes and the two-phonon $2D$ mode.[1] These second-order features, also referred to as double-resonant modes after Thomsen *et al.*,[11] involve nonzero phonon wave vectors q and can be described, to leading order, from fourth-order perturbation theory.[11–13]

The $2D'$ feature[1,2] seen in graphene and more generally sp^2 carbons is one such second-order Raman mode.[14] It arises from two phonons with nearly opposite wave vectors belonging to the LO branch of the phonon dispersion surrounding the $\mathbf{\Gamma}$ point. It is alternatively known as the G^* mode and is present at $\sim$3200 cm^{-1} for excitation energies in the visible range. Characteristic of its double-resonant nature,[11] the probed phonon wave vectors $\boldsymbol{q}^*$ move progressively away from $\mathbf{\Gamma}$ as the exciting laser energy is swept,[15] resulting in a dispersion of the observed mode frequency. This behavior evokes its more prominent foil, the $2D$ mode, that stems instead from the TO phonons around $\boldsymbol{K}$.[7,11] Theoretically too, the description of the $2D'$ feature mirrors that of the $2D$ mode, with the relevant Feynman diagrams[7,13,16,17] in both cases being identical save for the phonon branch considered ($2D'$:LO vs $2D$:TO). Unlike the $2D$ mode, however, the $2D'$ mode has not been subject to extensive experimental scrutiny. While a few reports have emerged regarding the investigation of its Grüneisen parameter,[9,18,19] its analyses under uniaxial strain, whether experimental or theoretical, particularly with regards to its polarization behavior are absent.

In this paper, we will show that polarization and laser energy E_L dependent measurements of the $2D'$ Raman mode of graphene provide access to the entire LO phonon dispersion of arbitrary radial and angular extent. This is in contrast to the oft-studied first-order Raman mode, the G mode, that is confined to $q \approx \Gamma$ independent of E_L.[20] We also provide the dominant phonon wave vectors $\boldsymbol{q}^*$ and the implied phonon-assisted electronic transitions associated with the $2D'$ mode, as a function of polarization. The LO phonon dispersion and the $2D'$ spectra are described under uniaxial and biaxial tension up to 2%. We study the behavior of the Grüneisen parameter $\gamma_{2D'}$ and the shear deformation potential $\beta_{2D'}$. While $\gamma_{2D'}$ is $\sim$5% less than γ_G, it also depends subtly on E_L. $\beta_{2D'}$, in contrast to β_G, exhibits a strong dependence on the polarizer:analyzer combination and the orientation ψ of uniaxial strain. Finally, relying only on the $2D'$ mode we suggest a robust technique to measure the level of uniaxial strain by rotating the plane of the polarizer and analyzer that are kept in a parallel configuration.

II. CALCULATION DETAILS

We model the $2D'$ Raman mode via a transition matrix $\mathcal{T}_{\mathrm{fi}}[\boldsymbol{q}]$[7] (the mode intensity $I_{2D'} \propto |\mathcal{T}_{\mathrm{fi}}[\boldsymbol{q}]|^2$) limited to fourth-order perturbation theory,[21] within the free-particle paradigm. It reads,

$$\mathcal{T}_{\mathrm{fi}}[\boldsymbol{q}] = \sum_k \frac{\langle v,k-q|H_{e-R}|c,k-q\rangle\langle v,k-q|H_{e-ph}|v,k\rangle^\dagger\langle c,k-q|H_{e-ph}|c,k\rangle\langle c,k|H_{e-R}|v,k\rangle}{\{E_L-(E_c[k-q]-E_v[k-q])-2\omega_{\mathrm{LO}}[q]+\imath\Gamma[E_L]\}\{E_L-(E_c[k-q]-E_v[k])-\omega_{\mathrm{LO}}[q]+\imath\Gamma[E_L]\}\{E_L-(E_c[k]-E_v[k])+\imath\Gamma[E_L]\}}$$
$$+\frac{\langle v,k-q|H_{e-R}|c,k-q\rangle\langle c,k-q|H_{e-ph}|c,k\rangle\langle v,k-q|H_{e-ph}|v,k\rangle^\dagger\langle c,k|H_{e-R}|v,k\rangle}{\{E_L-(E_c[k-q]-E_v[k-q])-2\omega_{\mathrm{LO}}[q]+\imath\Gamma[E_L]\}\{E_L-(E_c[k]-E_v[k-q])-\omega_{\mathrm{LO}}[q]+\imath\Gamma[E_L]\}\{E_L-(E_c[k]-E_v[k])+\imath\Gamma[E_L]\}}$$
$$+\frac{\langle v,k|H_{e-R}|c,k\rangle\langle c,k|H_{e-ph}|c,k-q\rangle\langle c,k-q|H_{e-ph}|c,k\rangle\langle c,k|H_{e-R}|v,k\rangle}{\{E_L-(E_c[k]-E_v[k])-2\omega_{\mathrm{LO}}[q]+\imath\Gamma[E_L]\}\{E_L-(E_c[k-q]-E_v[k])-\omega_{\mathrm{LO}}[q]+\imath\Gamma[E_L]\}\{E_L-(E_c[k]-E_v[k])+\imath\Gamma[E_L]\}}$$
$$+\frac{\langle c,k|H_{e-R}|v,k\rangle^\dagger\langle v,k|H_{e-ph}|v,k-q\rangle^\dagger\langle v,k-q|H_{e-ph}|v,k\rangle^\dagger\langle v,k|H_{e-R}|c,k\rangle^\dagger}{\{E_L-(E_c[k]-E_v[k])-2\omega_{\mathrm{LO}}[q]+\imath\Gamma[E_L]\}\{E_L-(E_c[k]-E_v[k-q])-\omega_{\mathrm{LO}}[q]+\imath\Gamma[E_L]\}\{E_L-(E_c[k]-E_v[k])+\imath\Gamma[E_L]\}},$$

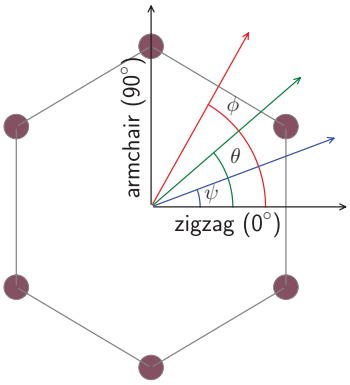

FIG. 1. (Color online) The angles corresponding to the polarizer θ, analyzer ϕ, and uniaxial strain orientation ψ with respect to the graphene lattice (purple circles). The axes are set along the zigzag and armchair orientations of graphene.

where H_{e-R} is the Hamiltonian corresponding to light-matter interaction and H_{e-ph} is the Hamiltonian representing electron-phonon coupling. The electronic eigenstates (for, e.g., $|c,k\rangle$) are labeled by their branch index (c: conduction band, v: valence band) and wave vector k. The band energies, as a function of the electronic wave vector k, are denoted by $E_v[k]$ and $E_c[k]$ for the valence and conduction bands of graphene, respectively, while the phonon dispersion, as a function of the phonon wave vector q, is $\omega_{\mathrm{LO}}[q]$. E_L is the incident laser energy and $\Gamma[E_L]$ is the energy broadening term. This perturbational approach has been used previously to study the $2D$ mode[7,13,22] to favorable correspondence with experiment.

The ingredient electronic and phonon bands and the associated optical and electron-phonon matrix elements were explicitly obtained over the entire two-dimensional Brillouin zone (BZ) of graphene via *ab initio* simulations. The electronic eigenfunctions were calculated in a plane-wave basis using density-functional theory (DFT)[23,24] within the local-density approximation (LDA),[25], as implemented in the QUANTUM ESPRESSO (QE)[26] distribution. We followed the established recipe of Ref. 8 in choosing the simulation parameters for the ground state wave functions of graphene, while suitably altering the lattice parameter for the biaxial strain case. For the uniaxial strain calculations, we proceeded by first finding the energy minima corresponding to the component of the lattice parameter perpendicular to the strain orientation in order to find the correct Poisson ratio ν. This was followed by the relaxation of the basis atoms to yield the eventual ground state. The optical matrix elements were computed while correcting for the nonlocality of the pseudopotentials used to generate the Kohn-Sham wave functions.[27] The electron-phonon matrix elements for the LO phonon branch were calculated using

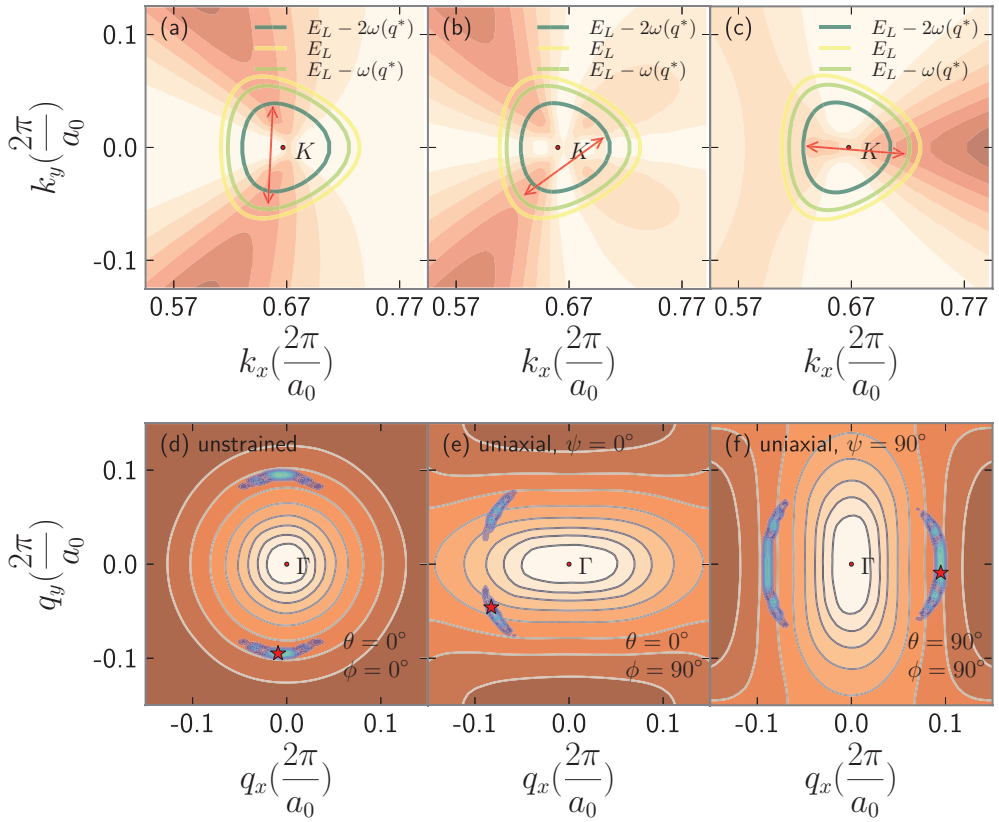

FIG. 2. (Color online) The phonon-assisted electronic transitions (red double-sided arrows) for (a) $\theta = 0°, \phi = 0°$, (b) $\theta = 0°, \phi = 90°$, and (c) $\theta = 90°, \phi = 90°$. They join the excitation energy contours $E_L - \omega_{\mathrm{LO}}(\boldsymbol{q}^*)$ and $E_L - 2\omega_{\mathrm{LO}}(\boldsymbol{q}^*)$, where the optical matrix elements product (underlying red-orange contours) is maximum. These transitions are implied by the dominant phonon wave vectors $\boldsymbol{q}^*$ (blue-green regions) probed by the $2D'$ Raman mode for the (d) pristine, (e) 1% uniaxially strained along the zigzag, and (e) 1% uniaxially strained along the armchair orientation cases. The underlying orange-hued contours of (d)–(f) depict the LO phonon dispersion around $\boldsymbol{\Gamma}$. The red stars represent the phonon wave vector with maximum intensity $\boldsymbol{q}^*_{\mathrm{max}}$.

the LDA wave functions by applying density-functional perturbation theory (DFPT).[28] Contrary to the optical laser energies (∼1.8 eV to 2.5 eV) commonly employed in Raman experiments, the laser energies E_L investigated were 1.3 eV to 1.9 eV, in order to confine ourselves to the domain of electronic wave vectors k probed by visible range irradiation. This is due to LDA's well-known underestimation of the slopes of both the electronic[29] and phonon bands[30] of graphene. A laser-dependent energy broadening $\Gamma[E_L]$ was used, as given by Eq. 14 of Ref. 22. $\mathcal{T}_{\rm fi}[\boldsymbol{q}]$ was calculated by carefully resampling the fully two-dimensional bands and matrix elements on a grid with a density exceeding 1000 × 1000 per BZ[31] for both the electronic k and phonon wave vectors q, ensuring converged results. Finally, the $2D'$ features were generated by modeling the spectrometric response by a Lorentzian profile with an FWHM of 1.5 cm^{-1}.

III. DOMINANT PHONONS q^* AND ELECTRONIC TRANSITIONS

Our calculations demonstrate that the dominant phonons $\boldsymbol{q}^*$ probed by the $2D'$ Raman mode are not confined to the high-symmetry directions, in general.[32] Instead, their location depends sensitively on light polarization as determined by the polarizer:analyzer condition (θ:ϕ) (see Fig. 1 for the definition of θ and ϕ). Their structure is very similar to $\boldsymbol{q}^*$ for the $2D$ mode obtained by us in Ref. 7. In Figs. 2(d)–2(f) we show $\boldsymbol{q}^*$ for representative polarizer:analyzer (θ:ϕ) combinations, where the polarization angle of 0° (90°) corresponds to the zigzag (armchair) orientation of the graphene lattice. Via the relation expressing quasimomentum conservation of the electron during phonon-assisted scattering, $\boldsymbol{k}_i^* = \boldsymbol{k}_f^* + \boldsymbol{q}^*$ and $\max(|\mathcal{T}_{\rm fi}[\boldsymbol{k}_i^*\boldsymbol{q}^*]|^2)$, $\boldsymbol{k}_f^*$ and $\boldsymbol{q}^*$ determine the dominant phonon-assisted transitions as shown by the red, double-sided arrows in Figs. 2(a)–2(c). These transitions connect regions where the product of the optical matrix elements are maximized, as set by (θ:ϕ). Given the resonant nature of the scattering process, one may intuit that the transitions simply connect the equiexcitation energy contours of the electronic dispersion ($E_c[k] - E_v[k] = E_L$), whereas on closer inspection we find that the strongest contributions come from the transitions connecting the equiexcitation energy contours with $E_L - \omega_{\rm LO}(\boldsymbol{q}^*)$ and $E_L - 2\omega_{\rm LO}(\boldsymbol{q}^*)$ as shown in Figs. 2(a)–2(c).

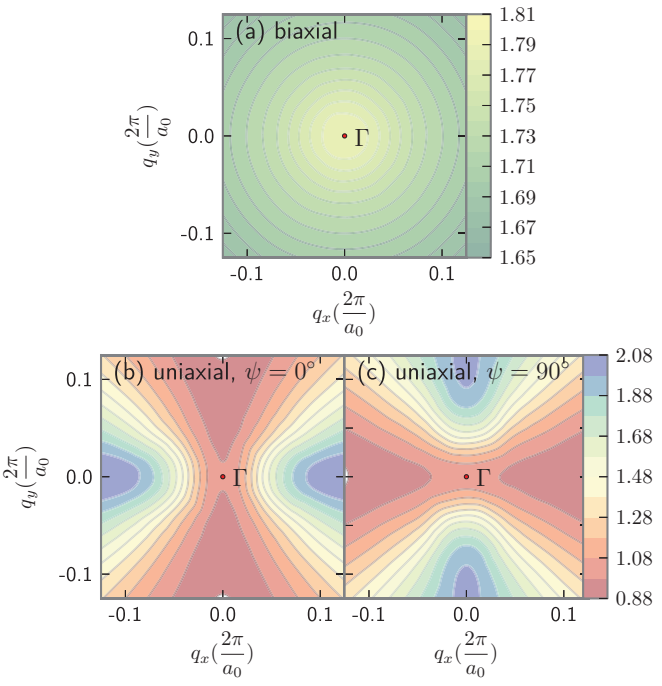

FIG. 3. (Color online) The differential strain response of the LO phonon branch of graphene around Γ under (a) biaxial strain $\gamma_{\rm LO} = -\frac{1}{2\omega_{\rm LO}^0}\frac{\partial\omega_{\rm LO}}{\partial\varepsilon_b}$ and uniaxial strain $-\frac{1}{\omega_{\rm LO}^0}\frac{\partial\omega_{\rm LO}}{\partial\varepsilon_u}$ along the (b) zigzag orientation ($\psi = 0°$) and (c) armchair orientations ($\psi = 90°$).

IV. STRAIN RESPONSE OF THE LO PHONON DISPERSION

Biaxial strain does not alter the D_{6v} (or D_6 when graphene is atop a substrate) point group symmetry of pristine graphene. The BZ remains hexagonal and the electron and phonon bands

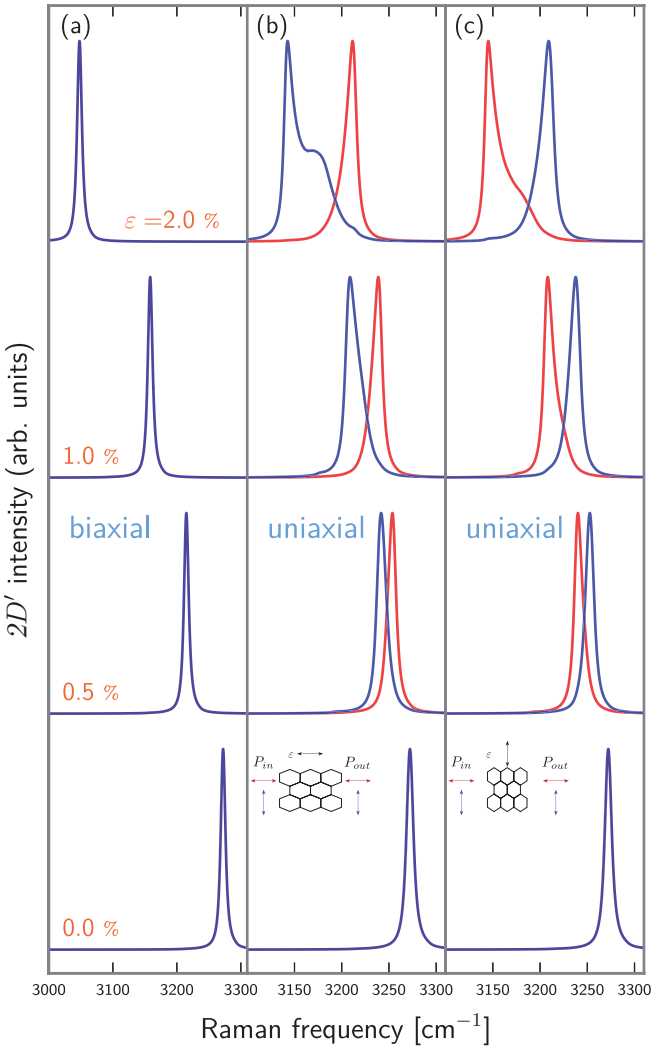

FIG. 4. (Color online) $2D'$ Raman spectra at $E_L = 1.5$ eV as function of (a) biaxial ε_b, (b) uniaxial strain ε_u along the zigzag ($\psi = 0°$), and (c) armchair ($\psi = 90°$) orientations of graphene for strains up to 2%.

of graphene under biaxial tension simply renormalize;[33] they both redshift. The differential response of the LO phonons under biaxial strain, $-\frac{1}{2\omega_{\rm LO}^0}\frac{\partial\omega_{\rm LO}}{\partial\varepsilon_b}$ [see Fig. 3(a)], tantamount to the Grüneisen parameter $\gamma_{\rm LO}$, shows a weak, nearly isotropic decline with $\boldsymbol{q}$ relative to Γ. Our finding is in good agreement with Ref. 33 that evaluated $\gamma_{\rm LO}$ along the high-symmetry directions Γ-K-M.

Uniaxial strains require the distortion of the hexagonal BZ of graphene.[7,34] The point group symmetry is reduced to C_2, while the mirror m symmetry is retained under uniaxial strain along the zigzag and armchair orientations. The equiexcitation energy contours [see Figs. 2(b) and 2(c) for uniaxial tensile strains of 1% along the zigzag and armchair orientations, respectively] shift[35] [see also Figs. 6(a) and 6(b)] and are subtly altered from their unstrained, trigonal shape; the BZ edges $\boldsymbol{K}$ and the minima of the Kohn anomalies no longer remain coincident.[7,36] The LO phonon dispersion around $\boldsymbol{\Gamma}$, on the other hand, distorts markedly in a manner characteristic of the strain orientation and magnitude. This is shown in Figs. 2(e) and 2(f) that display the LO phonon dispersion around $\boldsymbol{\Gamma}$ under uniaxial tensile strain of 1% along the zigzag and armchair orientations, respectively. The differential response of the LO phonons under uniaxial strain $-\frac{1}{\omega_{\rm LO}^0}\frac{\partial\omega_{\rm LO}}{\partial\varepsilon_u}$ is highly anisotropic as is evident from Figs. 3(b) and 3(c). These findings regarding the polarization dependence of $\boldsymbol{q}^*$ and the strain magnitude and direction dependent distortion of the probed LO phonons around $\boldsymbol{\Gamma}$ anticipate the richness of the $2D'$ Raman mode under uniaxial strain.

V. POLARIZED $2D'$ SPECTRA UNDER TENSION

The $2D'$ Raman mode maintains its shape but shifts to lower frequencies under biaxial tension ε_b, as shown in Fig. 4(a), for strains up to 2% for $E_L = 1.5$ eV. Expectedly, the line shape and position of the $2D'$ feature are indifferent to polarization, a consequence of the unbroken D_{6v} symmetry. Instead, under uniaxial strain and given polarization, the $2D'$ peak shows a characteristic broadening as the strain magnitude is increased. A further increase eventually leads to splitting with a complex line shape that cannot, in general, be satisfactorily fit to merely

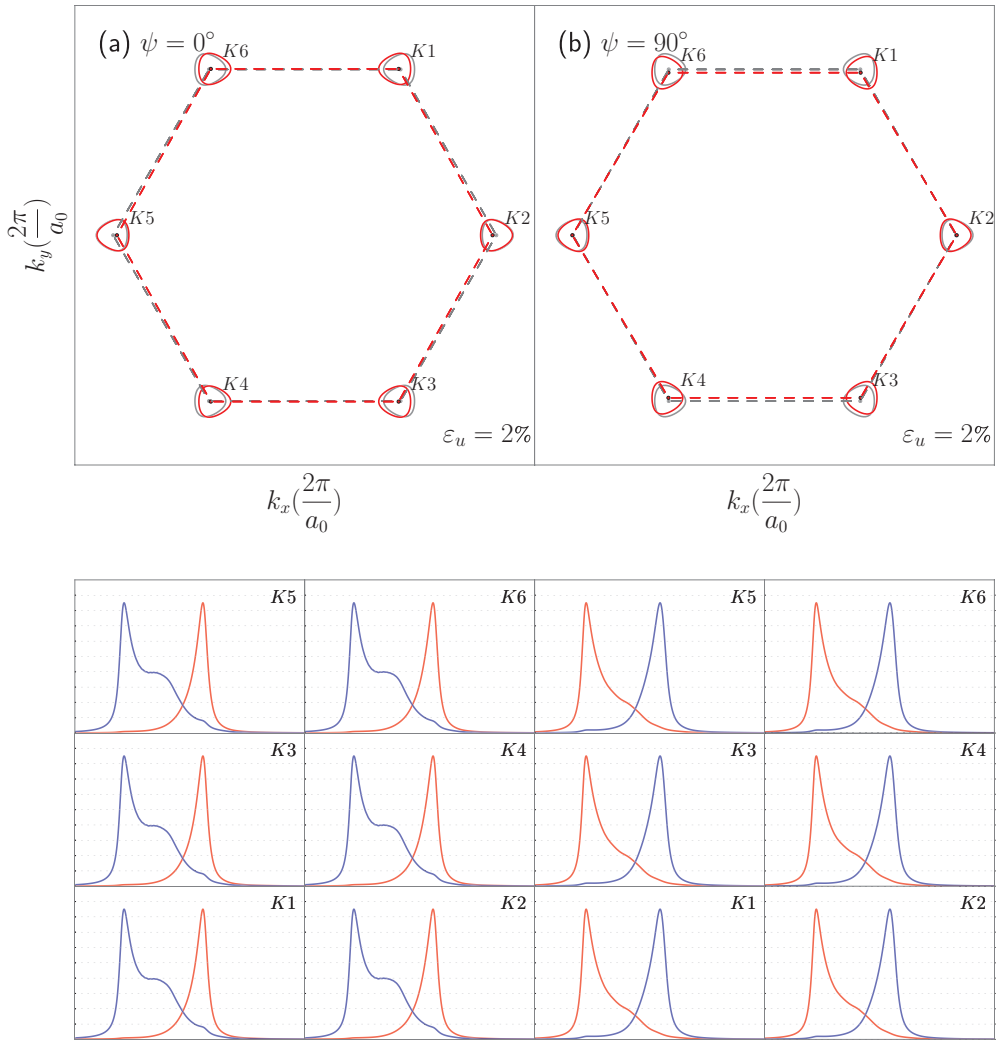

FIG. 5. (Color online) Top panels: The equienergy contours (in red) corresponding to the laser energy 1.5 eV for uniaxial strain $\varepsilon_u = 2.0\%$ along the (a) zigzag ($\psi = 0°$) and (b) armchair ($\psi = 90°$) orientations of the graphene lattice. They are contrasted with the contours (in gray) for unstrained graphene. Bottom panel: The $2D'$ Raman spectra (see the inset of Fig. 4 for the legend) derived from the individual BZ edges $\boldsymbol{K}i$, where i : 1–6. Given ψ, the $2D'$ spectra deriving from each Ki are identical.

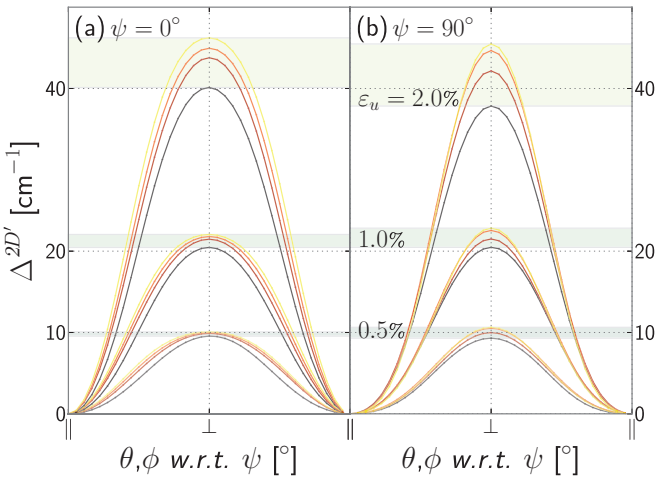

FIG. 6. (Color online) Variation of the intensity-weighted $2D'$ peak difference $\Delta^{2D'}$ with uniaxial strain ε_u along the (a) zigzag ($\psi = 0°$) and (b) armchair ($\psi = 90°$) orientations of the graphene lattice. The difference reaches a maximum $\Delta^{2D'}_{\parallel,\perp}$ when θ,ϕ are $\parallel$ and $\perp$ to ψ. $\Delta^{2D'}_{\parallel,\perp}$ provides a measure for ε_u.

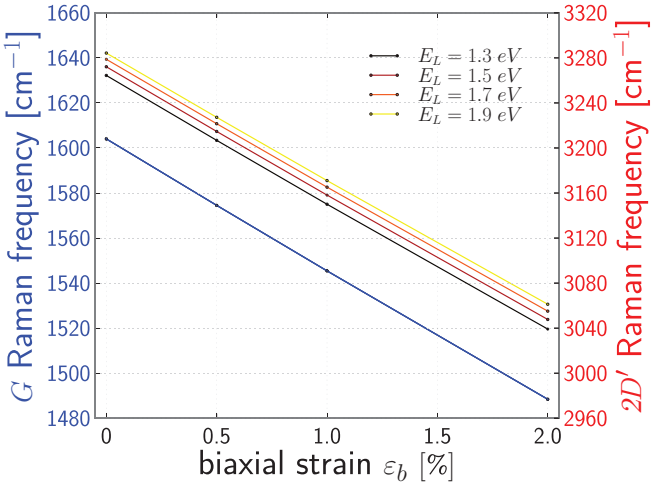

FIG. 7. (Color online) The intensity-weighted phonon frequency of the $2D'$ mode as a function of biaxial strain ε_b for various laser energies E_L. These are contrasted with the frequency of the G mode (blue line).

two Lorentzians. The line shape and peak positions are highly polarization (θ:ϕ) dependent, as exemplified by Figs. 4(b) and 4(c) for uniaxial strains along the (b) zigzag ($\psi = 0°$) and (c) armchair ($\psi = 90°$) orientations of the graphene lattice. It should be emphasized that the careful consideration of the polarizer:analyzer condition is not only of academic concern. Owing to the strong polarization dependence of standard spectrometer optics, paradoxically, a truly "unpolarized" experiment would rather be challenging to realize with crystalline specimens. The unreckoned polarization is probably at the heart of the higher scatter in the reported peak positions of the second-order but nevertheless prominent Raman features such as the $2D$ mode under strain.[18] The red (blue) peaks in Figs. 4(b) and 4(c) indicate a $\parallel$ ($\perp$) orientation of the polarizer and analyzer along the zigzag (armchair) orientation of graphene. Both the $\parallel$ and $\perp$ polarization conditions show a symmetry under exchange between $\psi = 0°$ and $\psi = 90°$ for small strains ($\sim$1%), that is somewhat lost at higher strain levels [compare Figs. 4(b) and 4(c) for $\varepsilon_u = 2.0\%$]. Generally, under uniaxial tension the peak with both θ and ϕ $\parallel$ ($\perp$) ψ develops a redshifted (blueshifted) shoulder, mirroring the behavior of the $2D$ mode seen experimentally[37,38] and in simulations.[7]

The observed line shape is primarily a consequence of the degree of parallelism between the polarization-dependent $\boldsymbol{q}^*$

TABLE I. Collected experimental and *ab initio* values for the Grüneisen parameter γ and shear deformation potential β of the G and $2D'$ modes of graphene.

			ab initio				experimental					*ab initio*		
			this work				Ref. 9	Ref. 18	Ref. 19	Ref. 39	Ref. 10	Ref. 9	Ref. 40	Ref. 41
E_L			1.3 eV	1.5 eV	1.7 eV	1.9 eV	2.43 eV	2.35 eV	2.43 eV	1.97 eV	2.34 eV			
γ_G				1.80			1.99	1.80	1.80	2.4 ± 0.2	0.69 ± 0.14	1.87	1.86	2.00
$\gamma_{2D'}$			1.72	1.71	1.70	1.69	1.74	1.73	$1.66 \pm 5\%$					
β_G							0.99				0.38 ± 0.08	0.92	0.96	0.66
$\beta_{G^-}[\psi]$														
0°				0.98					NA				NA	
90°				0.90					NA				NA	
$\beta_{G^+}[\psi]$														
0°				0.96					NA				NA	
90°				0.91					NA				NA	
$\beta_{2D'}[\psi,\theta.\phi]$														
0°	0°	0°	0.85	0.82	0.80	0.80								
0°	0°	90°	0.45	0.35	0.24	0.50								
0°	90°	90°	−0.25	−0.40	−0.49	−0.53			NA				NA	
90°	0°	0°	−0.32	−0.47	−0.57	−0.59								
90°	0°	90°	0.34	0.27	0.23	0.19								
90°	90°	90°	0.77	0.74	0.71	0.70								

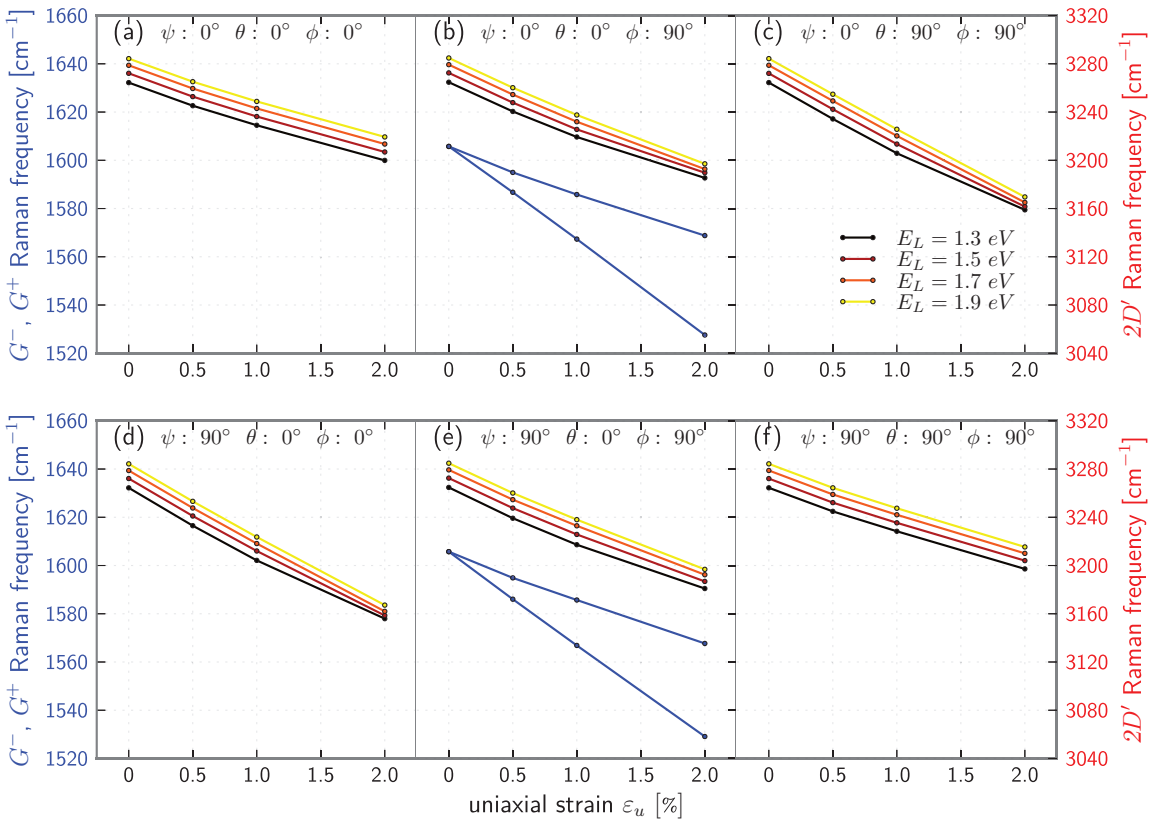

FIG. 8. (Color online) The intensity-weighted phonon frequency of the $2D'$ Raman mode as a function of uniaxial strain ε_u along the zigzag ($\psi = 0°$) [(a)–(c)] and armchair ($\psi = 90°$) orientations [(d)–(f)] for laser energies 1.3 eV (yellow line), 1.5 eV (orange line), 1.7 eV (red line), and 1.9 eV (black line). These are contrasted with the frequencies of the G^- and G^+ Raman modes (blue lines). The light polarization conditions are (a), (d) $\theta = 0°, \phi = 0°$, (b), (e) $\theta = 0°, \phi = 90°$, and (c), (f) $\theta = 90°, \phi = 90°$, where 0° corresponds to the zigzag orientation of graphene.

and the highly distorted LO phonon contours under uniaxial strain [see Figs. 2(e) and 2(f)]. In the limiting case of pristine (or biaxially strained) graphene, q^* are highly concordant with the LO phonon contours [see Fig. 2(d)] resulting thus in a narrow $2D'$ feature. The peak decomposition has little to do with the different relative motion of the individual BZ edges with respect to Γ. Indeed, under uniaxial strain along the zigzag and armchair directions, the electron valleys located at each of the six $\boldsymbol{K}$ points all yield identical $2D'$ line shapes (see Fig. 5).

The polarized $2D'$ spectra exhibit a maximum in the difference $\Delta^{2D'}$ between their peak positions (defined as the intensity-weighted spectral average of the $2D'$ Raman mode $\frac{\sum_q \omega_{2D'}[q] \times I_{2D'}[q]}{\sum_q I_{2D'}[q]}$), when $\theta, \phi \parallel \psi$ and $\theta, \phi \perp \psi$ as displayed in Figs. 6(a) and 6(b). This maximal difference $\Delta^{2D'}_{\parallel,\perp}$ serves as a measure of the magnitude of uniaxial tensile strain, once the laser energy E_L is kept constant. This is demonstrated by the position of maxima $\Delta^{2D'}_{\parallel,\perp}$ as a function of uniaxial strain ε_u in Fig. 6. Experimentally, we can exploit this fact to estimate the level of uniaxial strain by rotating the polarizer:analyzer, that are kept parallel to each other, through a 90° sweep to assess $\Delta^{2D'}_{\parallel,\perp}$. Indeed, Fig. 6 shows that for modest strains ($\varepsilon_u \sim 1\%$), $\frac{\partial \Delta^{2D'}_{\parallel,\perp}}{\partial \varepsilon_u} \approx 21$ cm^{-1}/%, regardless of ψ or E_L. As this method relies on the lowered symmetry of the graphene lattice under strain, it is therefore robust against the confounding effects of doping and/or the underlying substrate on the LO mode of graphene.

VI. GRÜNEISEN PARAMETER $\gamma_{2D'}$ AND SHEAR DEFORMATION POTENTIAL $\beta_{2D'}$

With the application of uniaxial strain the G Raman mode of graphene splits into the G^- and the higher frequency G^+ component.[9,10] Since both the G^+ and $2D'$ Raman features stem from the LO branch of the phonon dispersion of graphene,[9] we can reasonably expect a similar response to strain. We thus set the relation between the $2D'$ mode frequency $\omega_{2D'}$ and strain in correspondence with the G^+ mode as[9]

$$\omega_{2D'} = \omega^0_{2D'} - \gamma_{2D'}\omega^0_{2D'}\varepsilon_h + \tfrac{1}{2}\beta_{2D'}\omega^0_{2D'}\varepsilon_s, \tag{1}$$

where ε_h and ε_s denote the hydrostatic and shear components, respectively, of the strain tensor. The $2D'$ mode Grüneisen parameter is $\gamma_{2D'}$ while the shear deformation potential is $\beta_{2D'}$. For the case of biaxial strain ε_b we obtain

$$\omega_{2D'} = \omega^0_{2D'} - \gamma_{2D'}\omega^0_{2D'}(2\varepsilon_b), \tag{2}$$

whereas for a uniaxial strain ϵ_u we have

$$\omega_{2D'} = \omega^0_{2D'} - \gamma_{2D'}\omega^0_{2D'}\varepsilon_u(1-\nu) + \tfrac{1}{2}\beta_{2D'}\omega^0_{2D'}\varepsilon_u(1+\nu), \tag{3}$$

where ν is the Poisson ratio. $\gamma_{2D'}$ and $\beta_{2D'}$ are obtained from a linear regression following Eqs. (2) and (3), respectively, using the intensity-weighted phonon frequencies $\omega_{2D'}$ up to a strain level of 2% for both uniaxial and biaxial tension. A single Poisson ratio $\nu = 0.15$ is employed, which is the mean value from our calculations, in good accord with Ref. 10 and 40 and matches the one used in Ref. 9.

We find that (see Fig. 7) the Grüneisen parameter for the $2D'$ mode $\gamma_{2D'}^{1.5\ \mathrm{eV}} = 1.71$, which is $\sim 5\%$ less than that of the G mode with $\gamma_G = 1.80$, the latter being in good agreement with experimental and *ab initio* values as given in Table I. While comparing strain-response parameters between publications, one must be cognizant of the strain range considered. For instance, at higher strain the frequency-response of the G mode deviates from strict linearity, thus accounting, *ceteris paribus*, for the minor variation between reported values. The grossly discrepant γ_G value from Ref. 10, however, suggests a miscalibration of strain by a factor of three.[9,38] $\gamma_{2D'}$, in contrast to γ_G, shows a mild inverse dependence on the laser energy as can be observed from Fig. 7 and Table I. This reflects the double-resonant character of the $2D'$ mode, whereas the G mode is confined to $q \approx \Gamma$ where $\gamma_{\mathrm{LO}}[\Gamma] = 1.8$, regardless of the excitation energy [see Fig. 3(a)].

The response of the $2D'$ mode is considerably more nuanced when uniaxial tension is applied instead. It is strongly influenced by the polarization:analyzer condition (θ:ϕ) and ψ. (θ:ϕ) determines $\boldsymbol{q}^*$ for the LO phonons whose differential strain response [see Figs. 3(b) and 3(c)] is inherently highly anisotropic and ψ dependent. A weaker dependence on the laser energy E_L is also observed accounting for the fact that the double-resonant condition results in progressively larger $\boldsymbol{q}^*$ (than $\boldsymbol{\Gamma}$) being accessed as the excitation energy is swept upward. We present the intensity-weighted frequencies of the calculated $2D'$, G^-, and G^+ modes in Fig. 8 as a function of ε_u up to 2% along $\psi = 0°$, 90° with both θ, $\phi \parallel \psi$ and θ, $\phi \perp \psi$. Over a 2% uniaxial strain range, the obtained β_{G^+} and β_{G^-} are not identical and depend weakly on ψ as also discussed in Ref. 40. The nominal β_G is nevertheless in overall agreement with the literature values as tabulated in Table I. While the underestimated β_G from Ref. 10 can be attributed to the issue of strain calibration mentioned earlier, the origin of the discrepant value from Ref. 41 is suspected to be the lower strain level considered in that work. Using $\gamma_{2D'}$ from Eq. (2) in Eq. (3) we find that the inferred shear deformation potential $\beta_{2D'}$ is extremely sensitive to the (ψ, θ, ϕ) triad, and even changes sign, particularly when θ,$\phi \perp \psi$ [see Figs. 8(b) and 8(d)]. A weak dependence on E_L, for reasons given above, is also seen. Of note too is the reciprocity between the strain response of the $2D'$ mode between the cases: $\theta \parallel \phi \parallel \psi$ [compare Figs. 8(a) and 8(f)], $\theta \parallel \phi \perp \psi$ [compare Figs. 8(c) and 8(d)] and the $\theta \perp \phi \parallel$ (or $\perp$) ψ [compare Figs. 8(b) and 8(e)] for $\psi = 0°$,90°.

VII. CONCLUSIONS AND SUMMARY

We have shown that using a combination of polarization conditions (θ:ϕ) and laser energies E_L, the $2D'$ mode provides access to $\boldsymbol{q}^*$ of arbitrary radial[22] and even arbitrary angular locations relative to Γ [see Figs. 2(d)–2(f)]. It thus overcomes the restriction of the G mode (and the uniaxial strain induced G^+ mode) in being limited to probing the $q \approx \Gamma$ phonons of the LO branch. Whereas one might argue that the D' mode at $\sim$1620 cm^{-1} can perform the same task, it is usually difficult to study since it tends to get overshadowed by the G mode. The D' mode also suffers from the fact that it requires defects for its activation[1,22] and is therefore not guaranteed to have sufficient intensity. In this context, the $2D'$ mode becomes particularly valuable since it is located at $\sim$ 3200 cm^{-1}, well insulated from any interference.

Under biaxial tension the LO phonons redshift in a nearly isotropic manner about Γ [see Fig. 3(a)]. This is reflected in the Grüneisen parameter for the $2D'$ mode $\gamma_{2D'} \approx 1.70$, that is slightly laser dependent and roughly $\sim 5\%$ less than γ_G. The $2D'$ profile relocates to lower frequencies but shows no polarization dependence due to the unaltered symmetry of pristine graphene. Under uniaxial strain, the LO phonons distort markedly depending on the direction ψ along which the strain is applied and the magnitude of strain [see Figs. 3(b) and 3(c) for strains along the zigzag ($\psi = 0°$) and armchair ($\phi = 90°$) directions]. As a consequence, the $2D'$ profile is strongly polarization dependent as exemplified in Figs. 4(b) and 4(c). The shear deformation potential implied by the $2D'$ mode $\beta_{2D'}$ inherits the strong polarization dependence and even turns negative when $\theta \perp \phi$.

The intensity-averaged peak positions of the $2D$ mode show a maximum in the splitting $\Delta_{2D'}$ when the polarizer and analyzer, kept parallel to one other, are parallel and perpendicular, respectively, to the direction ψ along which the strain is applied. The maxima $\Delta_{\parallel,\perp}^{2D'}$ serve as a robust measure of uniaxial strain. For uniaxial strains up to 1% we find $\frac{\partial \Delta_{\parallel,\perp}^{2D'}}{\partial \varepsilon_u} \approx 21$ cm^{-1}/%, regardless of ψ or E_L. Experimentally, this maxima can be assessed by rotating the ($\theta \parallel \phi$) pair through 90° and providing a measure of uniaxial strain complementary to the splitting of the G^- and G^+ modes.[9,10]

ACKNOWLEDGMENTS

We thank Nicola Marzari and Nicola Bonini for useful comments. Parts of the work were supported by the European Research Council (ERC) under Grant No. 210642.

*narula@physik.fu-berlin.de

[1] S. Reich and C. Thomsen, Philos. Trans. R. Soc. A **362**, 2271 (2004).
[2] A. C. Ferrari *et al.*, Phys. Rev. Lett **97**, 187401 (2006).
[3] K. S. Novoselov *et al.*, Science **306**, 666 (2004).
[4] A. K. Geim and K. S. Novoselov, Nat. Mater. **6**, 183 (2007).
[5] S. Pisana *et al.*, Nat. Mater. **6**, 198 (2007).

[6]R. Saito, A. Jorio, A. G. Souza Filho, G. Dresselhaus, M. S. Dresselhaus, and M. A. Pimenta, Phys. Rev. Lett. **88**, 027401 (2001).
[7]R. Narula, N. Bonini, N. Marzari, and S. Reich, Phys. Rev. B **85**, 115451 (2012).
[8]N. Bonini, M. Lazzeri, N. Marzari, and F. Mauri, Phys. Rev. Lett. **99**, 176802 (2007).
[9]T. M. G. Mohiuddin *et al.*, Phys. Rev. B **79**, 205433 (2009).
[10]M. Huang *et al.*, Proc. Natl. Acad. Sci. **106**, 7304 (2009).
[11]C. Thomsen and S. Reich, Phys. Rev. Lett. **85**, 5214 (2000).
[12]R. Narula, Ph.D. thesis, Massachusetts Institute of Technology, 2011.
[13]D. M. Basko, Phys. Rev. B **78**, 125418 (2008).
[14]R. M. Martin and L. M. Falicov, in *Light Scattering in Solids II*, edited by M. Cardona and G. Guntherhodt (Springer-Verlag, Berlin, 1982).
[15]R. Narula and S. Reich, Phys. Rev. B **78**, 165422 (2008).
[16]J. Kürti, V. Zólyomi, A. Grüneis, and H. Kuzmany, Phys. Rev. B **65**, 165433 (2002).
[17]R. Narula, N. Bonini, N. Marzari, and S. Reich, Phys. Status Solidi B **248**, 2635 (2011).
[18]F. Ding *et al.*, Nano Lett. **10**, 3453 (2010).
[19]J. Zabel *et al.*, Nano Lett. **12**, 617 (2011).
[20]M. Cardona, in *Light Scattering in Solids II*, edited by M. Cardona and G. Guntherhodt (Springer-Verlag, Berlin, 1982).
[21]Given the resonant nature of the $2D'$ Raman mode, the contribution of terms of higher order in perturbation theory cannot *a priori* be neglected (Ref. 42).
[22]P. Venezuela, M. Lazzeri, and F. Mauri, Phys. Rev. B **84**, 035433 (2011).
[23]P. Hohenberg and W. Kohn, Phys. Rev. **136**, B864 (1964).
[24]W. Kohn and L. J. Sham, Phys. Rev. **140**, A1133 (1965).
[25]D. M. Ceperley and B. J. Alder, Phys. Rev. Lett. **45**, 566 (1980).
[26]P. Giannozzi *et al.*, J. Phys.: Condens. Matter **21**, 395502 (2009).
[27]A. F. Starace, Phys. Rev. A **3**, 1242 (1971).
[28]S. Baroni, S. de Gironcoli, A. Dal Corso, and P. Giannozzi, Rev. Mod. Phys. **73**, 515 (2001).
[29]A. Gruneis, C. Attaccalite, L. Wirtz, H. Shiozawa, R. Saito, T. Pichler, and A. Rubio, Phys. Rev. B **78**, 205425 (2008).
[30]M. Lazzeri, C. Attaccalite, L. Wirtz, and F. Mauri, Phys. Rev. B **78**, 081406 (2008).
[31]A two-dimensional interpolation of the ingredient matrix elements and energy bands was performed first in k space and subsequently in q space using standard routines that are part of the SciPy package (Ref. 43). The $\mathcal{T}_{\rm fi}[\boldsymbol{q}]$ corresponding to each q were calculated separately using a self-created parallel code written in PYTHON.
[32]Venezuela *et al.* (Ref. 22) considered the idealized situation of an unpolarized Raman experiment.
[33]N. Mounet and N. Marzari, Phys. Rev. B **71**, 205214 (2005).
[34]M. Mohr, K. Papagelis, J. Maultzsch, and C. Thomsen, Phys. Rev. B **80**, 205410 (2009).
[35]The shift referred to here occurs in the reciprocal space with coordinates scaled to the lattice parameter a_0 of pristine graphene.
[36]V. M. Pereira, A. H. Castro Neto, and N. M. R. Peres, Phys. Rev. B **80**, 045401 (2009).
[37]M. Huang, H. Yan, T. F. Heinz, and J. Hone, Nano Lett. **10**, 4074 (2010).
[38]O. Frank *et al.*, ACS Nano **5**, 2231 (2011).
[39]C. Metzger *et al.*, Nano Lett. **10**, 6 (2009).
[40]Y. C. Cheng, Z. Y. Zhu, G. S. Huang, and U. Schwingenschlögl, Phys. Rev. B **83**, 115449 (2011).
[41]C. Thomsen, S. Reich, and P. Ordejón, Phys. Rev. B **65**, 073403 (2002).
[42]C. Cohen-Tannoudji, J. Dupont-Roc, and G. Grynberg, *Atom-Phonon Interactions: Basic Processes and Applications* (John Wiley & Sons, New York, 1992).
[43]E. Jones *et al.*, SciPy: Open source scientific tools for PYTHON, 2001.